International Journal of Robotics and Control Systems
Vol. 3, No. 4, 2023, pp. 780-803
ISSN 2775-2658
http://pubs2.ascee.org/index.php/ijrcs

Identification and Control of Epidemic Disease Based Neural Networks and Optimization Technique

Ahmed J. Abougarair [a,1,*], Shada E. Elwefati [b,2]

[a] Electrical and Electronics Engineering, University of Tripoli, Tripoli, Libya
[b] Biomedical Engineering, University of Tripoli, Tripoli, Libya
[1] a.abougarair@uot.edu.ly; [2] shada.wefati@gmail.com
* Corresponding Author

ARTICLE INFO

Article history
Received September 04, 2023
Revised October 04, 2023
Accepted October 15, 2023

Keywords
ANN;
Epidemiology;
SIR Model;
PMP;
RNN

ABSTRACT

Developing effective strategies to contain the spread of infectious diseases, particularly in the case of rapidly evolving outbreaks like COVID-19, remains a pressing challenge. The Susceptible-Infected-Recovery (SIR) model, a fundamental tool in epidemiology, offers insights into disease dynamics. The SIR system exhibits complex nonlinear relationships between the input variables (e.g., population, infection rate, recovery rate) and the output variables (e.g., the number of infected individuals over time). We employ Recurrent Neural Networks (RNNs) to model the SIR system due to their ability to capture sequential dependencies and handle time-series data effectively. RNNs, with their ability to model nonlinear functions, can capture these intricate relationships, enabling accurate predictions and understanding of the dynamics of the system. Additionally, we apply the Pontryagin Minimum Principle (PMP) based different control strategies to formulate an optimal control approach aimed at maximizing the recovery rate while minimizing the number of affected individuals and achieving a balance between minimizing costs and satisfying constraints. This can include optimizing vaccination strategies, quarantine measures, treatment allocation, and resource allocation. The findings of this research indicate that the proposed modeling and control approach shows potential for a comprehensive analysis of viral spread, providing valuable insights and strategies for disease management on a global level. By integrating epidemiological modeling with intelligent control techniques, we contribute to the ongoing efforts aimed at combating infectious diseases on a larger scale.

1. Introduction

The field of epidemiology, which focuses on the patterns and dynamics of diseases within populations, plays a crucial role in comprehending and tackling infectious diseases. This field has become increasingly essential as new theories and explanations for epidemics emerge [1]. Since the emergence of COVID-19 in early 2020, the world has faced an unprecedented challenge characterized by an atypical pneumonia outbreak. COVID-19 not only poses a significant threat to public health but also exerts substantial economic pressure worldwide. The complexities of diagnosing and treating COVID-19 present formidable challenges for healthcare professionals. The foundation of modern epidemiological modeling traces back to the pioneering work of Kermack and McKendrick, who introduced compartmental epidemic models, including the Susceptible-Infection-Recovery (SIR) and

Susceptible-Exposed-Infectious-Recovery (SEIR) models [2]. The SIR model, particularly suited for simulating diseases that confer lifelong immunity post-recovery, remains a primary choice in infectious disease modeling [3]. In the realm of parameter identification for epidemic models, traditional computation offers two primary approaches: least squares-based methods [4] and gradient-based methods [5]. While these methods have proven effective in various applications, they are not without limitations. Least squares methods struggle with time-variant parameters, while gradient-based methods often require heuristic gain adjustments to achieve convergence. Recognizing these limitations is crucial when selecting parameter identification strategies, as alternative methods may be necessary to ensure accuracy, especially when dealing with dynamic parameters or convergence challenges [6]. Artificial Neural Networks (ANNs) emerge as valuable tools for enhancing the diagnosis of COVID-19. ANNs offer the potential to improve diagnostic accuracy and speed, facilitating timely screening, treatment, and vigilant monitoring. This study leverages Recurrent Neural Networks (RNNs) to propose an estimation method for epidemic models, benefiting from the network's optimization capabilities. Notably, RNNs eliminate the need for heuristic gain adjustments, drawing inspiration from gradient-based approaches. Previous applications of this neural network estimation technique have yielded promising results in other domains, such as robotics [7]. Preliminary investigations with real data have also shown promise [8]-[9]. Our primary objective is to present an efficient and versatile neural network-based approach for elucidating human control strategies within epidemic disease models. We seek a neural network architecture capable of modeling dynamic SIR systems effectively [10]. Furthermore, optimal control theory offers a robust mathematical framework for effectively managing and mitigating the spread of a wide range of diseases. Optimal control involves determining the best trajectory for a dynamic system through time, considering state and input controls, to minimize or maximize a performance index [11]-[12]. The Pontryagin Minimum Principle (PMP), a cornerstone of optimal control theory, aids in determining the optimal path for transitioning the SIR model from one state to the next, particularly when constraints are imposed on state or input controls [13]. The remainder of this paper is organized as follows: Section 2 introduces the mathematical tools in Real-World Disease Control and Prevention . Section 3 delves into the control methodology, and Section 4 presents simulation results. Section 5 showcases the graphical user interface (GUI) for SIR optimal control strategies, and Section 6 concludes our study.

2. Mathematical Tools in Real-World Disease Control and Prevention

Mathematical tools play a crucial role in real-world disease control and prevention by offering quantitative frameworks and computational methods. These tools assist in evidence-based decision-making, optimize control strategies, analyze data, forecast disease trends, and allocate resources effectively. By enhancing our understanding of epidemic dynamics and supporting policy development, mathematical tools contribute to more efficient and effective public health interventions.

2.1. Mathematical Model of SIR

The last few years have seen a significant increase in interest in epidemic mathematical models inside various formal frameworks [14]-[15]. Some of these models are expressed using dynamic systems, control theory, differential, difference, and hybrid equations [16]-[23], information theory, [24], etc. Modeling infectious illnesses is a fascinating area of mathematical biology. The models give a clear framework for understanding biological systems and their infections [25]-[26]. Thus, the development of a nonlinear system of ODE, which served as the basis for SIR and SEIR, marked the beginning of compartmental epidemic modeling [27]. Mathematical models are useful tools in many fields of biology, including ecology, evolution, toxicology, immunology, and natural resource management biology. Biological theory is tested and expanded upon using the findings from the analysis and simulation of epidemic models, which also serve as a basis for new hypotheses and studies. Numerous works on epidemiological modeling take into account deterministic modeling, which categorizes the population into classifications called compartments according to their epidemiological status, such as susceptible, infected, and recovering [28]. In this paper, we will

develop the SIR model, which is an epidemiological model designed to estimate the projected number of cases of an infectious disease within a confined community as time progresses. In the SIR model, it is assumed that individuals mix uniformly and have an equal likelihood of encountering each other, leading to an equal probability of infection for everyone. However, in reality, contact patterns can differ considerably due to factors like geographical location, social networks, and individual behaviors. Additionally, the SIR model assumes that the parameters governing disease transmission and recovery remain fixed throughout the epidemic. This assumption suggests that the disease dynamics and population characteristics do not undergo any changes over time. In actuality, the effectiveness of interventions, population behavior, and pathogen evolution can affect these parameters [29]. The SIR model as shown in Fig. 1 is a widely used mathematical framework in epidemiology to study the dynamics of infectious diseases. In this model, the population is divided into three groups: susceptible (S), infected (I), and recovered (R). Here's an explanation of the significance of each parameter and variable in the SIR model [29].

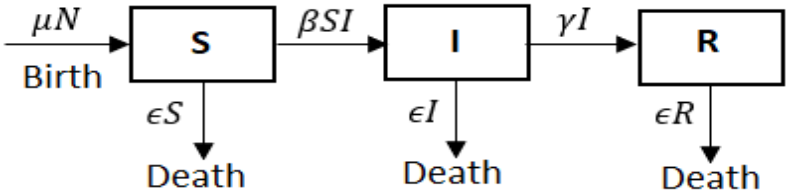

Fig. 1. SIR model without control [1], [29]

- Susceptible population (S)
  This variable represents the number of individuals who have not been infected and are susceptible to contracting the disease.
- Infected population (I)
  This variable represents the number of individuals who are currently infected and can transmit the disease to susceptible individuals.
- Recovered population (R)
  This variable represents the number of individuals who have recovered from the infection and have developed immunity, either through treatment or by surviving the disease. Recovered individuals are no longer susceptible to reinfection and cannot spread the disease.
- Transmission rate (β)
  This parameter quantifies the speed at which the infection spreads from infected individuals to susceptible individuals. It depends on factors such as the contagiousness of the disease, contact patterns among individuals, and preventive measures in place.
- Recovery rate (γ)
  This parameter represents the rate at which infected individuals recover from the disease and transition into the recovered compartment. It is the inverse of the average duration of the infection. A shorter recovery rate implies a faster recovery and a shorter period of infectiousness.

The reason for including demographic factors like births and deaths caused by the disease in the SIR model is to consider how population changes influence the transmission and development of infectious diseases. By integrating demographic factors, the model becomes more holistic, allowing for a better grasp of disease dynamics and their potential long-term consequences [30]-[31].

The following presumptions are taken in the epidemiological SIR model presented here, which also takes into account the SIR epidemic model with demography [29]. We also have an additional equation where N is the entire population and must not change.

$$N(t) = S(t) + I(t) + R(t) \quad (1)$$

The initial state conditions are $S(0) \geq 0, I(0) \geq 0, and\ R(0) \geq 0$ and $S(t_f), I(t_f), and\ R(t_f) = free\ final\ states$. Where the infection and recovery rates are represented by $\beta > 0$ and $0 < \gamma < 1$, respectively. Typically, we use S(0), I(0), and R(0) as the beginning conditions as the first observational data, and we assume that the entire population N is time-invariant for analysis.

$\dot{N}(t) = \dot{S}(t) + \dot{I}(t) + \dot{R}(t) = 0\mu$ and $\epsilon \in [0, 1]$ are, respectively, births and deaths due to disease. The equations of the SIR model are [29]-[30]:

$$\dot{S}(t) = \mu N - \frac{\beta S(t) I(t)}{N} - \epsilon S(t), \quad S(0) = S_0 \tag{2}$$

$$\dot{I}(t) = \frac{S(t) I(t)}{N} - \gamma I(t) - \epsilon I(t), \quad I(0) = I_0 \tag{3}$$

$$\dot{R}(t) = \gamma I(t) - \epsilon R(t), R(0) = R_0 \tag{4}$$

The population is N(t), and its derivative over time can be calculated by $\dot{N}(t) = \dot{S}(t) + \dot{I}(t) + \dot{R}(t)$

$$\dot{N}(t) = \mu N - \frac{S(t) I(t)}{N}(\beta + 1) - \epsilon(S(t) - I(t)) \tag{5}$$

$N(0) = N_0 = S_0 + I_0 + R_0$ at equilibrium points, the SIR model's parameters do not alter over time, i.e. [30]. $\dot{S}(t) = \dot{I}(t) = \dot{R}(t) = 0$. So, we can rewrite (2) and (3) as assuming tiny value of μ, and ϵ about equal to zero.

$$\dot{S}(t) = 0 \approx -\beta \frac{S I}{N} \tag{6}$$

$$\dot{I}(t) = 0 \approx \frac{S(t) I(t)}{N} - \gamma I(t) \tag{7}$$

Assume $f_1(S, I) = \frac{dS}{dt} and\ f_2(S, I) = \frac{dI}{dt}$. The Jacobian matrix A as in the following form [31]. By substitute equilibrium point $(S = N, I = 0)$. Then, calculate the eigenvalues from,

$$\mathrm{A} = \begin{bmatrix} \frac{\partial f_1}{\partial S} & \frac{\partial f_1}{\partial I} \\ \frac{\partial f_2}{\partial S} & \frac{\partial f_2}{\partial I} \end{bmatrix} = \begin{vmatrix} -\frac{\beta I}{N} & -\frac{\beta S}{N} \\ \frac{\beta I}{N} & \frac{\beta S}{N} - \gamma \end{vmatrix} = \begin{bmatrix} 0 & -\beta \\ 0 & \beta - \gamma \end{bmatrix} \tag{8}$$

$$|r\, I - A| = 0 \rightarrow \begin{vmatrix} r & -\beta \\ 0 & r - \beta + \gamma \end{vmatrix} = r(r - \beta + \gamma) = 0 \tag{9}$$

These two eigenvalues are provided $r = 0$, and $r = \beta - \gamma$ In general, the eigenvalue $r = 0$ neglect it (because it is not practical). Where classification of the equilibrium point (r_1 and r_2 are the two eigenvalues of A) are:

- $r_1, r_2 > 0$ unstable node
- $r_1, r_2 < 0$ stable node
- $r_1 > 0, r_2 < 0$ saddle point

So with eigenvalue $r = \beta - \gamma$, have two solutions if $r = \beta - \gamma > 0$, the solution grows away from the equilibrium, the equilibrium is unstable. For the SIR model, this is an epidemic. If $r = \beta - \gamma < 0$, the solution contract back towards the equilibrium. The equilibrium is stable. For the SIR model, this is no epidemic.

2.2. Neural Networks Identification

The System Identification (SI) method uses observed input-output data to approximate a system's model. One of the most crucial factors to consider before designing a controller is system

identification. The suggested method employs a back propagation neural network (NN) to anticipate the system's output for a new input based on previous inputs and outputs [32]-[33]. The use of neural networks in epidemic modeling aims to harness their capabilities in capturing intricate patterns and connections within the data. Neural networks, including Recurrent Neural Networks (RNNs), excel at processing extensive information, handling sequential data, and effectively modeling nonlinear relationships. Epidemic data typically involves the disease's progression over time, making neural networks, particularly RNNs, well-suited for modeling time-series data and capturing the temporal dependencies and dynamics of the epidemic. By employing neural networks, we can effectively capture complex and nonlinear relationships among various factors like population demographics, transmission rates, and intervention measures. This approach facilitates a more comprehensive understanding of the intricate interactions and complexities associated with disease spread. The RNN is depicted in Fig. 2 with n inputs, t outputs, and m hidden layer nodes. The input, internal state, and output vector of the network are each represented by u, z, and y, respectively [34].

$$\begin{Bmatrix} u(k) = [u_1(k) \ \dots \ u_n(k)]^T \\ z(k) = [z_1(k) \ \dots \ z_m(k)]^T \\ \hat{y}(k) = [\hat{y}_1(k) \ \dots \ \hat{y}_t(k)]^T \end{Bmatrix} \tag{10}$$

The equations of the network are

$$\begin{Bmatrix} z(k) = \psi\big(Wu(k) + Sz(k-1)\big) \\ \hat{y}(k) = Vz(k) \end{Bmatrix} \tag{11}$$

ψ is the tangent hyperbolic function and is the activation function of the interior layer neurons.

$$\psi(x) = tanh(x) = \frac{e^x - e^{-x}}{e^x + e^{-x}} \tag{12}$$

Where W $m \times n$, S $m \times m$, and V $t \times m$ are weight matrices

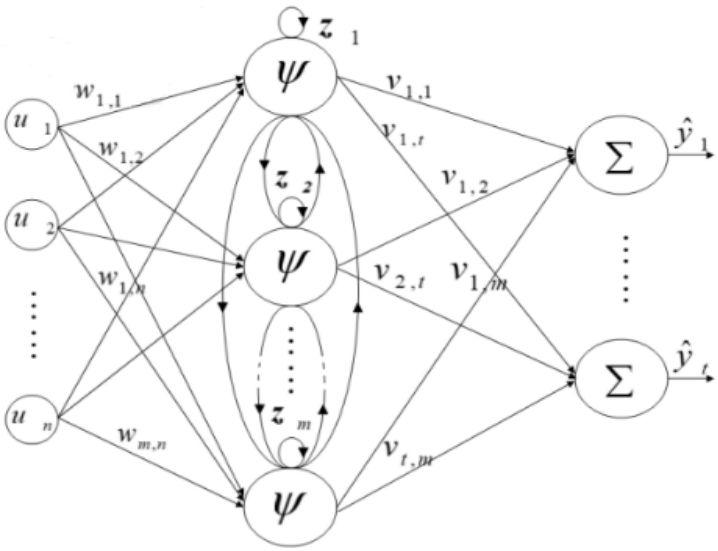

Fig. 2. Neural network structure [32]

The training process for a neural network entail presenting it with input data along with the corresponding expected output. The network then adapts its internal parameters, referred to as weights and biases, to reduce the disparity between its output and the desired output. Backpropagation is employed to propagate the error backwards through the network. This technique involves calculating the gradients of the loss function with respect to the weights and biases of each neuron. These gradients indicate the direction and magnitude of adjustments needed to minimize the prediction error. The network's weights and biases are subsequently updated in accordance with the computed gradients

using an optimization algorithm, such as gradient descent. The Mean Square Error (MSE) provides as the cost function, for N is the number of training samples. y is the actual output and $\hat{y}$ is the predicted output of neural network.

$$MSE = \frac{1}{N}\sum_{k=1}^{N} e(k)^T . e(k) \tag{13}$$

$$MSE = \frac{1}{N}\sum_{k=1}^{N} (\hat{y}(k) - y(k))^T . (\hat{y}(k) - y(k)) \tag{14}$$

The selection of network architecture, including the number of neurons in the hidden layer and the choice of activation functions, is influenced by several factors, such as the problem's complexity, computational resources available, and prior knowledge about the data. Having too few neurons may result in underfitting, where the network fails to capture complex patterns in the data. Conversely, an excessive number of neurons can lead to overfitting, where the network overly memorizes the training data instead of learning generalizable patterns. The selection of activation functions is dependent on the problem's nature and the specific characteristics of the data [34]-[35].

In our model, the RNN based on the SIR network model contains two different states of the number of neurons in the hidden layer where in the first case five neurons were used and in the second case twenty neurons, with tan activation functions in each case and three saturated linear functions were used in the output layer as shown in Fig. 3.

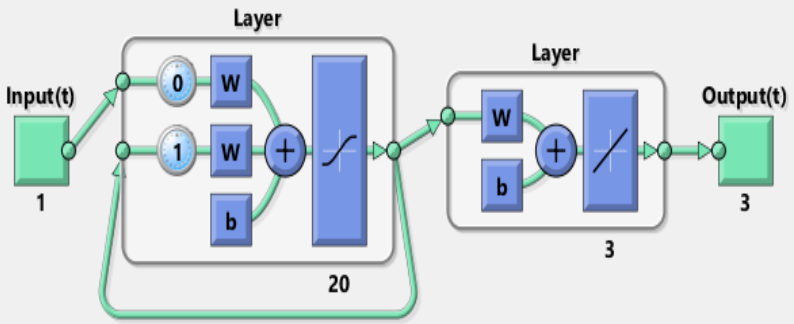

Fig. 3. Neural network structure of SIR model

The selection of 5 and 20 neurons in the hidden layer could have been determined by conducting experiments and validation on the particular problem and dataset. These specific configurations might have been identified as a suitable balance between model complexity and generalization, leading to satisfactory performance in terms of prediction accuracy while avoiding issues of overfitting or underfitting. The input and output data sets used for training are obtained by numerical solution for differential equations of SIR model. The first offline batch Levenberg-Marquadt optimization network training is done [32]. The prediction error is the networks. Therefore, the algorithm's main goal is to reduce the prediction error over the training set of data. The results that show the neural network model for five and twenty neurons in hidden layer predicted outputs versus the actual SIR model outputs are shown in Fig. 4 and Fig. 5 respectively. At this point, the optimal network weights for network (20 neuron in hidden layer) are stored and used for validation [33]-[35]. The model is trained using the training vectors repeatedly until the training successfully decreases network error to the desired outcome. The MSE squared error starting at a large value and decreasing to a small value as shown in Fig. 6, where three lines make up the plot, representing the training, validation, and test phases. After 416 training iterations, the cost function is minimized to the order of 4.5×10^{-9}.

Validation involves utilizing both the training and test datasets to assess the degree of alignment between the neural identification model and the numerically obtained data. This process provides insights into the accuracy and closeness of fit between the model and the actual data.

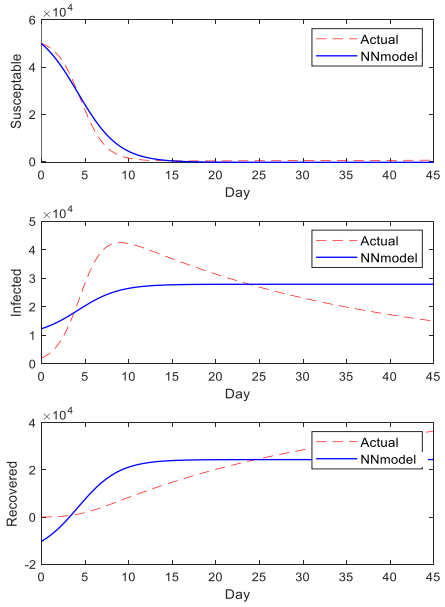

Fig. 4. Outputs of actual SIR model with outputs of NN model based 5 neurons in hidden layer

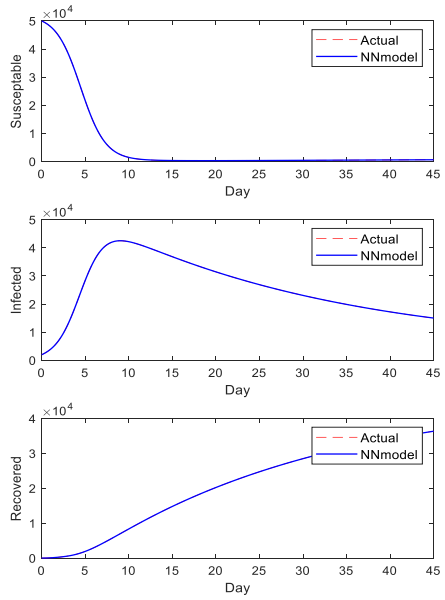

Fig. 5. Outputs of actual SIR model with output of NN model based 20 neurons in hidden layer

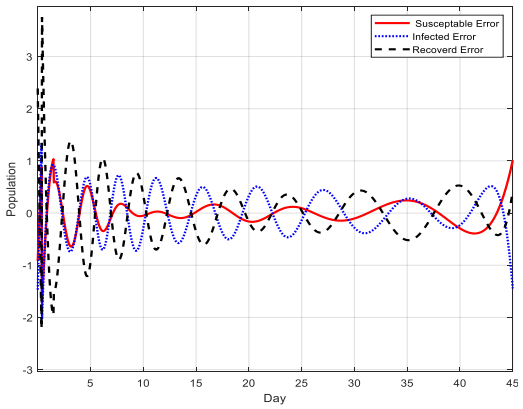

Fig. 6. MSE of NN base 20 neurons in hidden layer

Fig. 7 shows the difference between the actual values and the estimated values for all states of the SIR system using neural networks if 20 neurons are used in the hidden layer. Table 1 presents the MSE for susceptible, infection and recovery respectively, based 20 neurons neural network model. The obtained result demonstrates that neural networks can be used effectively for the identification of SIR model. The validation results for the susceptible output are depicted in Fig. 8, illustrating that the prediction error over the training data is minimal.

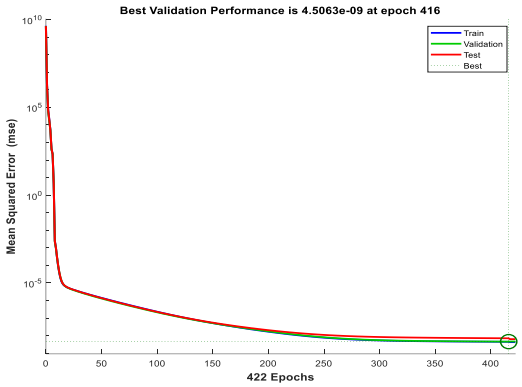

Fig. 7. Difference between actual and predicted states

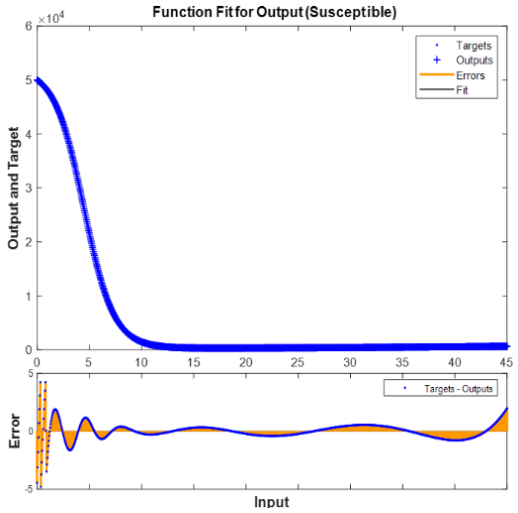

Fig. 8. Function fit for susceptible case

Table 1. MSE of SIR model-based 20 neurons NN

Susceptible	Infection	Recovery
0.0677	0.1716	0.3149

Fig. 9 displays the error histogram with 20 bins for the three neural network modeling processes of training, validation, and testing. The quantity of samples from the dataset that fall into each vertical bar's respective bin is shown. In the Fig. 9 presented, a yellow line in the center represents a zero error, indicating 350 instances within the training set. In the middle of the plot, there is a bin that corresponds to an error of 1.56×10^{-6}. The height of this bin for the training dataset is slightly below 225, indicating that around 225 samples in the training dataset have errors falling within this range. Additionally, both the validation and test datasets fall between the range of 225 and 325, suggesting that a significant number of samples from different datasets have errors within this specific range.

Also, linear regression analysis is the most standard method to test the performance of a NN model. Here the neural network output and the corresponding data set target for the testing

instances are plotted as shown in Fig. 10. From the simulation results, the correlation coefficient is very close to 1, we can say that the neural network predicts the SIR model very well.

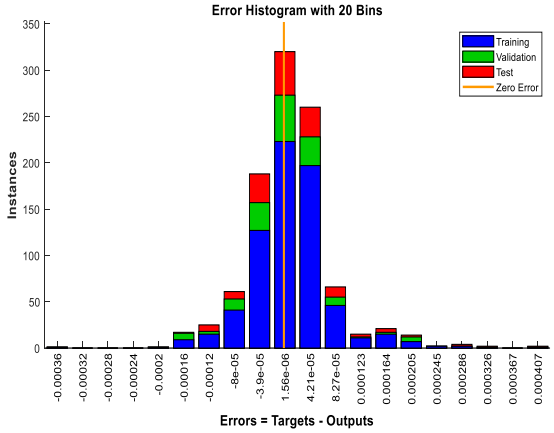

Fig. 9. Histogram with 20 bins for the training, validation, and test in NN model

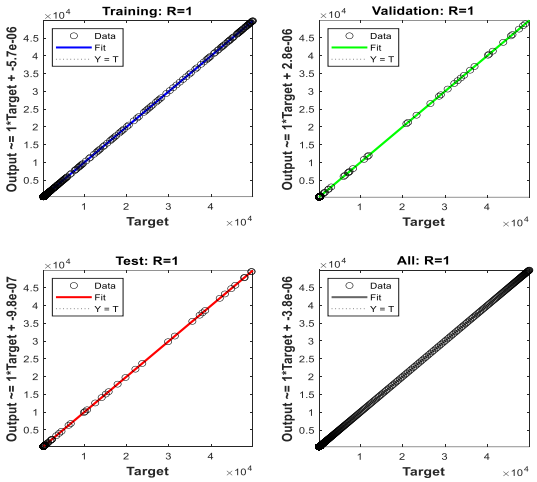

Fig. 10. Test data for Validation neural model

2.3. Optimal Control Strategies

Optimal control strategies are crucial in managing epidemics as they are vital for implementing efficient interventions, optimizing the allocation of resources, reducing disease transmission, ensuring cost-effectiveness, enabling timely decision-making, facilitating long-term planning, and adapting to changing circumstances. These strategies offer a systematic and evidence-based approach to minimizing the impact of infectious diseases on public health and society as a whole. Optimal control strategies are beneficial in curtailing the transmission of infectious diseases by employing measures like vaccination campaigns, quarantine protocols, contact tracing, social distancing, and travel restrictions.

These strategies aim to decrease contact rates and restrict the spread of the disease among the population. Optimal control strategies, also aid in efficiently distributing scarce resources like healthcare facilities, medical supplies, and personnel. Through strategic resource management, these strategies ensure that healthcare systems are well-equipped to handle a surge in cases, deliver suitable treatment, and alleviate strain on the healthcare infrastructure [35]-[36]. In this section, we investigate the behavior of the SIR model using optimal control theory. To design and implement optimal control strategies, we employ the PMP, which is commonly used for obtaining optimal control strategies in continuous processes. Various mathematical techniques exist for solving optimal control problems. The following explanation outlines how these techniques can be applied to solve simpler problems. The PMP steps are illustrated in the flowchart presented in Fig. 11, [29], [37].

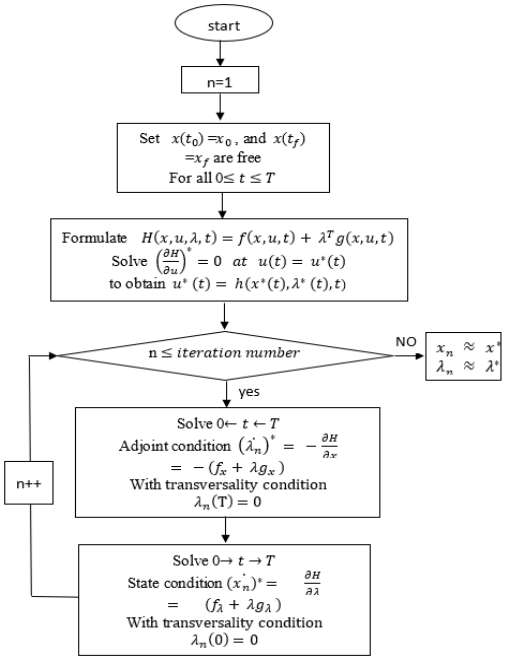

Fig. 11. Flowchart of the PMP steps [29]

1. Construct the problem's Hamiltonian equation.

$$H(x(t),u(t),\lambda(t),t)=f(x(t),u(t),t)+\lambda^T g(x(t),u(t),t) \tag{15}$$

Where, $H(t,x,u,\lambda)$ is a Hamilton equation, $f(x(t),u(t),t)$. $g(x(t),u(t),t)$ are based on state, control, and tim. $\lambda^T(t)$ is a vector of costate vector of n[th] order

2. Differentiation Hamilton's equation to get the optimal control u^*(t)

$$H(x(t),u(t),\lambda(t),t)=f(x(t),u(t),t)+\lambda^T g(x(t),u(t),t) \tag{16}$$

To obtain $u^*(t)=$ h$(x^*(t),\lambda^*(t),t)$. Here h$(x^*(t),\lambda^*(t),t)$ represents a function that depends on the optimal states, optimal control, and time.

3. Find H^* using optimal control signal u^*.

$$H^*(x^*(t),\text{h}(x^*(t),\lambda^*(t),t),\lambda^*(t),t)=H^*(x^*(t),\lambda^*(t),t) \tag{17}$$

4. Find the solution to the set of differential equations and the adjoint condition.

$$(\dot{\lambda})^*=-\left(\frac{\partial H}{\partial x}\right)^* \rightarrow (\dot{\lambda})^*=-(f_x+\lambda g_x) \tag{18}$$

The differentiation of the f and g in relation to the state x is indicated by the symbols f_x , g_x. With transversality condition, $\lambda(t_f)=0$ and transversality condition, $\lambda(0)=0$. The state equation, the differentiation of the f and g in relation to the adjoint λ is indicated by the symbols f_λ, g_λ.

$$(\dot{x})^*=\left(\frac{\partial H}{\partial \lambda}\right)^* \rightarrow (\dot{x})^*=(f_\lambda+\lambda g_\lambda) \tag{19}$$

Transversality conditions play a crucial role in optimal control problems by incorporating endpoint constraints, which define the desired behavior or conditions at the final time point. By satisfying these conditions, the optimal control solution ensures that the system reaches the desired endpoint consistently and appropriately. Moreover, transversality conditions transform the optimal

control problem into a boundary value problem. This conversion enables the utilization of mathematical techniques and algorithms specifically designed for solving boundary value problems. By formulating the problem in terms of both initial and final conditions, the transversality conditions provide a comprehensive depiction of the system dynamics [38]-[39].

5. Using MATLAB program to find the optimal control (u*) after determining the ideal states (x^*) and adjoint (λ).

When studying Hamiltonian equations and optimal control solutions within the context of managing epidemics, they offer valuable understanding about the most efficient approaches to mitigate disease transmission. The optimal controls signify the dynamic interventions or actions that are recommended to be implemented at different time points to minimize the spread of the disease. These controls encompass diverse measures, including vaccination rates, quarantine protocols, social distancing measures, or a combination of these strategies [40]-[41].

3. Control Strategies

The control strategies discussed in the paper hold significant importance, particularly within the field of epidemic models. Their primary objective is to effectively manage and reduce the transmission of infectious diseases, which is crucial in real-world scenarios with significant implications for public health. By implementing these control strategies, several benefits can be attained, including disease containment, resource allocation, decision support, and proactive planning. In conclusion, the investigation of these control strategies in the paper contributes to the advancement of evidence-based approaches to epidemic management, providing valuable insights and practical applications for addressing public health challenges [42]-[46].

3.1. Strategy 1 (Treatment Control)

This technique uses SIR model equations with a control strategy that is represented by control u in Fig. 12. After the control signals are added, the system equations will take on the new form shown below [29], [47], [48].

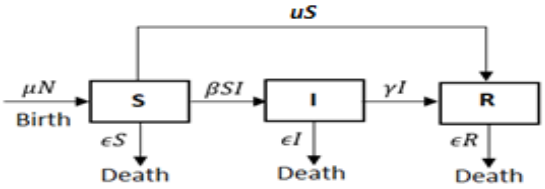

Fig. 12. SIR model with Treatment Control control u

$$\begin{cases} \dot{S}(t) = \mu N - \dfrac{\beta SI}{N} - \epsilon S - uS, & S(0) \geq 0 \\ \dot{I}(t) = \dfrac{\beta SI}{N} - \gamma I - \epsilon I, & I(0) \geq 0 \\ \dot{R}(t) = \gamma I - \epsilon R + uS, & R(0) \geq 0 \end{cases} \tag{20}$$

uS stands for the optimal control, which maximizes the performance index with the goal of lowering the number of sick individuals, the time of recovery, and the treatment expense. The following is a representation of the performance index.

$$J_1 = min \int_0^{t_f} \left[I(t) + w_1 \frac{u^2(t)}{2} \right] . dt \tag{21}$$

Where $w_1 \frac{u^2(t)}{2}$ defines the cost of the therapy, $w_1 \geq 0$ balances the cost variables and reflects the "weight" of the cost, and t_f denotes the length of the treatment period. The goal is to use the optimal possible control u^* to reduce the number of infected people and the cost of treatment.

$$J(u^*) = \min\{ J(u): u \in U \} \tag{22}$$

The set of admissible controls U defined by, $U = \{ u(t): 0 \leq u \leq u_{max}, t \in [0, t_f]$. The following steps are required when applying the Pontryagin principle method to the SIR model in order to execute an optimal control. Hamiltonian equation is:

$$H = (I + 0.5\, W\, u^2) + \dot{S}\, \lambda_1 + \dot{I}\, \lambda_2 + \dot{R}\lambda_3 \tag{23}$$

And $\frac{\partial \mathrm{H}}{\partial \mathrm{u}} = 0 \rightarrow \frac{\partial \mathrm{H}}{\partial \mathrm{u}} = Wu - \lambda_1 S + \lambda_3 S = 0$. By solving the Hamilton equation of equation to obtain u^*,

$$u^* = \frac{S(\lambda_1 - \lambda_3)}{W} \tag{24}$$

The adjoint equations can be obtained by such that $\dot{\lambda_1} = -\frac{\partial H}{\partial S}$, $\dot{\lambda_2} = -\frac{\partial H}{\partial I}$ and $\dot{\lambda_3} = -\frac{\partial H}{\partial R}$.

$$\left\{ \begin{array}{c} \dot{\lambda_1} = -\left(\frac{-\lambda_1 \beta I}{N} - \lambda_1 u + \frac{\lambda_2 \beta I}{N} + \lambda_3\, u + \epsilon \lambda_1\right) \\ \dot{\lambda_2} = -(1 - \lambda_1 \beta S + \lambda_2 \beta S - \lambda_2 \gamma + \lambda_3 \gamma + \epsilon \lambda_2) \\ \dot{\lambda_3} = \epsilon \lambda_3 \end{array} \right\} \tag{25}$$

The transversality conditions for free problem cases apply to this system, which is a free final state problem $\lambda_1(t_f) = \lambda_2(t_f) = \lambda_3(t_f) = 0$.

3.2. Strategy 2 (Vaccination Control)

The goal of the SIR model with control in the immunization control method is to increase recovery rates while minimizing the number of vulnerable, infected, and healing times. The efficiency index determined as [29], [49], [50].

$$J_2 = min \int_0^{t_f} \left[A_1 S(t) + A_2 I(t) - A_3 R(t) + W_2 \frac{u^2(t)}{2} \right] . dt \tag{26}$$

$A_1, A_2, and\ A_3$ are balancing cost factors, and the negative sign on A_3 is to minimize recovery people in the shortest amount of time, where $W_2 \frac{u^2(t)}{2}$ is indicating a cost of vaccination, the coefficient $W_2 \geq 0$ is balancing cost factors signals the "weight" on cost. The goal is to use the best possible control to reduce the number of susceptible and infected people, the cost of vaccination, and to increase the number of people who recover in the quickest time possible $J(u^*) = \min\{ J(u): u \in U \}$.

The set of admissible controls defined by $U = \{ u(t): 0 \leq u \leq u_{max}, t \in [0, t_f]$. The following steps, which combine the PMP and SIR models, must be taken in order to perform an optimal control. The Hamiltonian formula is:

$$H = \left(A_1 S(t) + A_2 I(t) + A_3 R(t) + \frac{W u^2(t)}{2} \right) + \dot{S}\, \lambda_1 + \dot{I}\, \lambda_2 + \dot{R}\lambda_3 \tag{27}$$

and

$$\frac{\partial \mathrm{H}}{\partial \mathrm{u}} = 0 \rightarrow \quad \frac{\partial \mathrm{H}}{\partial \mathrm{u}} = Wu - \lambda_1 S + \lambda_3 S \tag{28}$$

To obtain u*, the Hamilton equation is solved,

$$u^* = \frac{S(\lambda_1 - \lambda_3)}{W} \tag{29}$$

The adjoint equations can be obtained by such that $\dot{\lambda_1} = -\frac{\partial H}{\partial S}$, $\dot{\lambda_2} = -\frac{\partial H}{\partial I}$ and $\dot{\lambda_3} = -\frac{\partial H}{\partial R}$.

$$\begin{Bmatrix} \dot{\lambda_1} = -(A_1 - \beta I\lambda_1 - u\lambda_1 + \lambda_2\beta I + \lambda_3 u + \epsilon\lambda_1) \\ \dot{\lambda_2} = -(A_2 - \beta S\lambda_1 - \gamma\lambda_2 + \beta S\lambda_2 + \lambda_3\gamma + \epsilon\lambda_2) \\ \dot{\lambda_3} = A_3 + \epsilon\lambda_3 \end{Bmatrix} \tag{30}$$

In the context of this system, we encounter a free final state problem that involves the application of transversality conditions specific to free problem cases $\lambda_1(t_f) = \lambda_2(t_f) = \lambda_3(t_f) = 0$.

3.3. Strategy 3 (Susceptible Control)

The objective functional which can be used to minimize number of susceptible individuals, time of recover, and cost of vaccination is [29], [51], [52]:

$$J_3 = min \int_0^{t_f} \left[B\,S(t) + W_3 \frac{u^2(t)}{2} \right] . dt \tag{31}$$

In the given context, $W_3 \frac{u^2(t)}{2}$ represents the cost associated with vaccination, while B is a factor that balances the proportion of susceptible individuals. The objective function aims to minimize the cost of vaccination and reduce the number of susceptible individuals. This is achieved by determining the optimal control u^* that satisfies the given conditions $J(u^*) = \min\{J(u): u \in U\}$. The admissible controls U defined by, $U = \{u(t): 0 \le u \le u_{max}, t \in [0, t_f]$. The Hamiltonian formula is:

$$H = \left(BS(t) + \frac{Wu^2(t)}{2} \right) + \dot{S}\,\lambda_1 + \dot{I}\,\lambda_2 + \dot{R}\lambda_3 \tag{32}$$

and

$$\frac{\partial \mathrm{H}}{\partial \mathrm{u}} = 0 \rightarrow \frac{\partial \mathrm{H}}{\partial \mathrm{u}} = Wu - \lambda_1 S + \lambda_3 S \tag{33}$$

To obtain u*, the Hamilton equation is solved,

$$u^* = \frac{S(\lambda_1 - \lambda_3)}{W} \tag{34}$$

The adjoint equations can be obtained by such that $\dot{\lambda_1} = -\frac{\partial H}{\partial S}$, $\dot{\lambda_2} = -\frac{\partial H}{\partial I}$ and $\dot{\lambda_3} = -\frac{\partial H}{\partial R}$. In this particular system, we are dealing with a free final state problem that involves the application of transversality conditions specific to cases where the final state is unconstrained $\lambda_1(t_f) = \lambda_2(t_f) = \lambda_3(t_f) = 0$.

$$\begin{Bmatrix} \dot{\lambda_1} = -(\mathrm{B} - \beta I\lambda_1 + \lambda_2\beta I - \lambda_1 u + \epsilon\lambda_1 + \lambda_3 u) \\ \dot{\lambda_2} = -(-\beta S\lambda_1 - \gamma\lambda_2 + \beta S\lambda_2 + \lambda_3\gamma + \epsilon\lambda_2) \\ \dot{\lambda_3} = +\epsilon\lambda_3 \end{Bmatrix} \tag{35}$$

3.4. Strategy 4 (Quarantine and Vaccination Control)

This approach uses SIR model equations as shown in Fig. 13 with the controls u_1, u_2. The function that optimizes the performance index has parameters u_1, u_2 that represent the optimal controls [29], [53], [54].

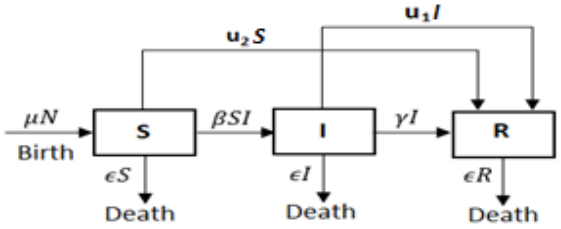

Fig. 13. SIR model with control u_1 and u_2

- $u_1 I$: depicts quarantine, the method of controlling contaminated people
- $u_2 S$: represents the quarantine that is used to regulate diseased people

In this case the number of infected individuals, time of recover, and cost of vaccination and quarantine, can be minimized using the following objective function.

$$J_4 = min \int_0^{t_f} \left[CI(t) + W_{41} \frac{u_1^2(t)}{2} + W_{42} \frac{u_2^2(t)}{2} \right] dt \tag{36}$$

The weight is indicated by the coefficients W_{41} and $W_{42} > 0$, which are balancing cost factors. $W_{42} \frac{u_2^2(t)}{2}$ stands in for the cost of quarantine where $W_{41} \frac{u_1^2(t)}{2}$stands for the cost of immunization, and C is a balancing to numbers of infected individuals. The goal is to use the best controls ${u_1}^*, {u_2}^*$ to reduce the cost of vaccination and quarantine while also reducing the number of infected people $J({u_1}^*, {u_2}^*) = \min\{ J(u_1, u_2): u_1, u_2 \in U \}$.

The admissible controls U defined by $U = \{ u_1, u_2(t): 0 \leq u_1, u_2 \leq u_{max}, t \in [0, t_f]$. The Hamiltonian formula is.

$$H = \left(C\, I(t) + W_1 \frac{u_1^2(t)}{2} + W_2 \frac{u_2^2(t)}{2} \right) + \dot{S}\, \lambda_1 + \dot{I}\, \lambda_2 + \dot{R} \lambda_3 \tag{37}$$

And

$$\left\{ \begin{matrix} \frac{\partial \mathrm{H}}{\partial u_1} = 0 \rightarrow \frac{\partial \mathrm{H}}{\partial u_1} = W_1 u_1 - \lambda_2 I + \lambda_3 I \\ \frac{\partial \mathrm{H}}{\partial u_2} = 0 \rightarrow \frac{\partial \mathrm{H}}{\partial u_2} = W_2 u_2 - \lambda_1 S + \lambda_3 s \end{matrix} \right\} \tag{38}$$

To obtain ${u_1}^*$ and $u_2^*$the Hamilton equation is solved,

$$\left\{ \begin{matrix} {u_1}^* = \frac{I(\lambda_2 - \lambda_3)}{W_1} \\ {u_2}^* = \frac{S(\lambda_1 - \lambda_3)}{W_2} \end{matrix} \right\} \tag{39}$$

The adjoint equations can be obtained by such that:

$$\left\{ \begin{matrix} \dot{\lambda_1} = -(-\beta I \lambda_1 + \lambda_2 \beta I - \lambda_1 u_2 \\ +\lambda_3 u_2 + \epsilon \lambda_1) \\ \dot{\lambda_2} = -(C - \beta S \lambda_1 - \gamma \lambda_2 + \beta S \lambda_2 + \lambda_2 u_1 + \lambda_3 \gamma \\ +\lambda_3 u_1 + \epsilon \lambda_2) \\ \dot{\lambda_3} = + \epsilon \lambda_3 \end{matrix} \right\} \tag{40}$$

The system at hand represents a free final state problem that necessitates the consideration of transversality conditions [55]-[56], $\lambda_1 (t_f) = \lambda_2 (t_f) = \lambda_3 (t_f) = 0$.

4. Simulation Results

Table 2 displays the COVID-19 data's numerical values. The total value of β is treated as an average value when performing analysis. While the value of γ is kept very low, Table 3 also shows the ideal control weights for each strategy.

Table 2. COVID -19 Data [29], [54]

β	γ	μ	ϵ	T	S_0	I_0	R_0
0.47/ (Days. People)	0.343 /Days	0.0007	0.0007	45 Days	75% People	20% People	5% People

Table 3. Disease optimal control weights [29]

Strategy (1)	$W_1 = 2$
Strategy (2)	$W_2 = 1$, $A_1 = 0.5$, $A_2 = 0.25$ $A_3 = 0.13$
Strategy (3)	$W_3 = 1.5$, $B = 0.1$
Strategy (4)	$W_{41} = 1$, $W_{42} = 0.5$, $C = 0.025$

In the realm of COVID-19 control, β, γ, and control weights play crucial roles in comprehending and managing the spread of the disease. A higher β signifies a more contagious virus, resulting in rapid spread and larger outbreaks. It is vital to grasp and estimate β to evaluate the impact of interventions like social distancing, mask-wearing, and vaccination in reducing transmission rates. Estimating γ aids in comprehending the natural progression of the disease, determining outbreak durations, and calculating indicators such as the primary reproduction number, which denotes the number of new infections caused by each infected individual among a susceptible population. Control weights pertain to the relative significance or effectiveness assigned to different control measures or interventions. In the context of COVID-19, control weights can indicate the impact of diverse measures like lockdowns, testing, contact tracing, vaccination, and public health guidelines. By assigning appropriate control weights, effectiveness of various interventions can be quantified, allowing for optimized control strategies. Mathematical models can incorporate these weights to assess the collective impact of multiple interventions, facilitate decision-making, and prioritize resources to achieve maximum disease control [57]-[58].

As shown in Fig. 14, the dynamic behavior of the system is examined using numerical simulation with no controls. The primary issue is that the population of susceptible individuals is growing over time. We will investigate the impact of altering some factors on system performance in order to accurately comprehend the system. To illustrate their effects, the simulation is run as a function of the β and γ.

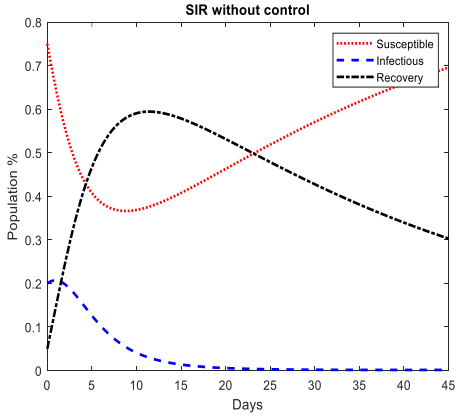

Fig. 14. Dynamic behavior of the SIR model without control

Using change β and γ, the following simulation results are produced. Fig. 15 illustrates the impacts of changing the recovery rate factor (γ=0.1, 0.067 and 0.033) when the spreading rate is low

(β=0.1). It is obvious that when the γ factor is low, the number of infected persons increases and the diseased people take a long time to recover. The number of affected people falls as the rate of recovery rises. Fig. 16 demonstrates how the number of vulnerable individuals is dramatically decreased when the spreading rate is increased to (β = 0.9), where (γ=0.1, 0.067, and 0.033). Due to the increased number of infected people and the longer recovery times, a high recovery rate factor is necessary to quicken the healing process.

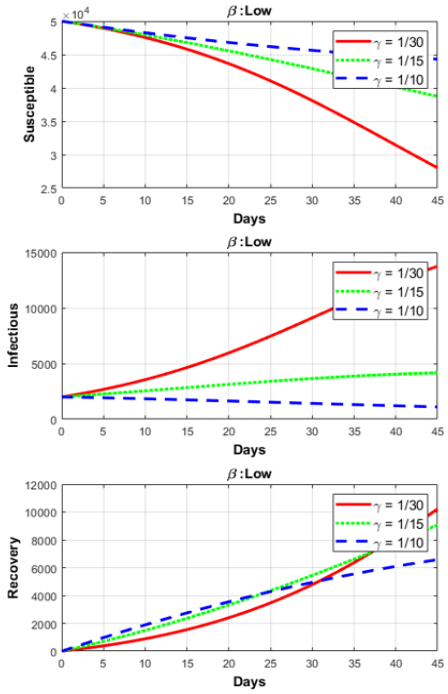

Fig. 15. SIR model characterized for β = 0.1

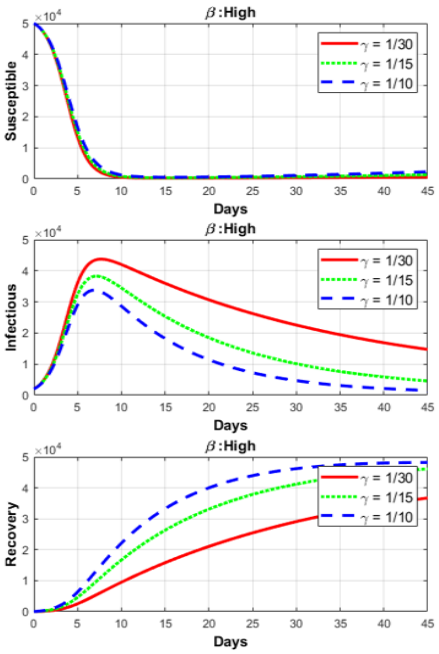

Fig. 16. SIR model characterized for β = 0.9

A higher or lower value of β indicates a corresponding increase or decrease in the likelihood of disease transmission. This parameter is influenced by various factors, including the disease's infectivity, the nature of contact between individuals, and the implementation of preventive measures

like mask usage and social distancing. β is a significant parameter as it directly affects the intensity and spread of the epidemic. Similarly, a higher or lower value of γ signifies a faster or slower rate of recovery, respectively. γ is influenced by factors such as the effectiveness of treatments, the natural progression of the disease, and an individual's immune response. This parameter plays a crucial role in determining the duration of an individual's infectious period and consequently affects the overall duration of the epidemic. To summarize, β reflects the contagiousness of the disease and governs the transmission rate, while γ represents the recovery rate and influences the duration of infection. Understanding these parameters is crucial for comprehending how the model simulates epidemic dynamics, as they directly impact the spread and control of infectious diseases.

In the subsequent analysis, the SIR model is subjected to four distinct control strategies, and a comparative evaluation is performed based on the simulation results. Fig. 17 illustrates that strategy (2) outperforms the other strategies by effectively reducing the number of susceptible individuals and preventing their infection. Furthermore, Fig. 18 demonstrates the impact of all control strategies on the number of infected individuals. It is evident that strategy (2) successfully mitigates the spread of infection, bringing the number of infected individuals to an acceptable level within the initial ten-day period.

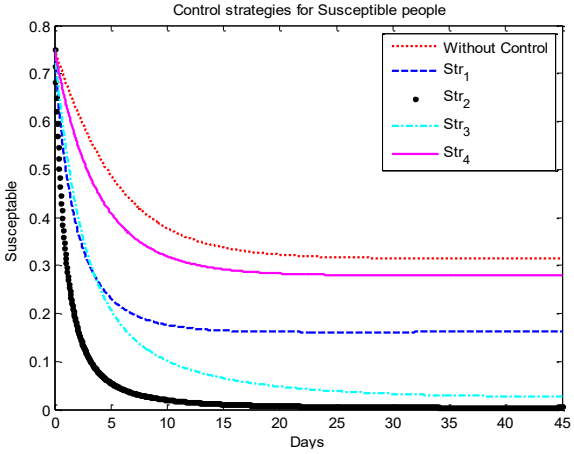

Fig. 17. Susceptible individuals with control strategies

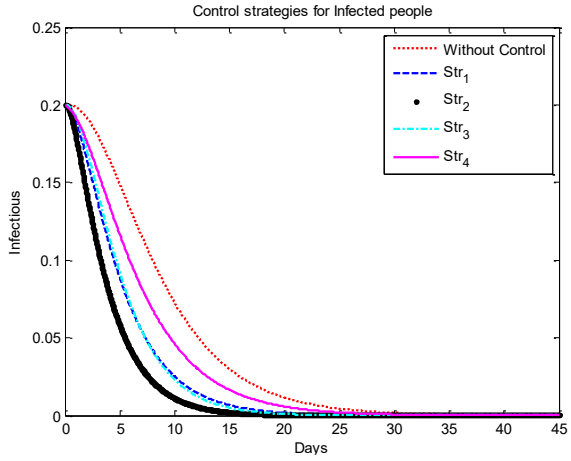

Fig. 18. Infected individuals with control strategies

Fig. 19 highlights the observable improvements and shorter recovery period achieved by strategy (2) compared to the other approaches. This emphasizes the superiority of immunization over medical intervention. Notably, strategy (2) has a significantly higher number of individuals in recovery between day 0 and day 45, indicating its effectiveness in minimizing the recovery time. In contrast, Fig. 20 shows that strategy (2) is not as effective in terms of cost minimization. Strategies (1) and (4)

perform better in terms of reducing costs compared to the other strategies. It is worth mentioning that the global community is actively searching for an efficient control strategy to swiftly contain and prevent the rapid spread of epidemics, as evident in the race to develop a vaccine for COVID-19.In conclusion, the simulation results demonstrate the effectiveness of strategy (2) in reducing susceptibility, preventing infection, and achieving shorter recovery periods. However, strategies (1) and (4) excel in cost minimization. The priority remains on safeguarding human lives, as evidenced by the urgent scientific efforts to develop vaccines and control measures for COVID-19.

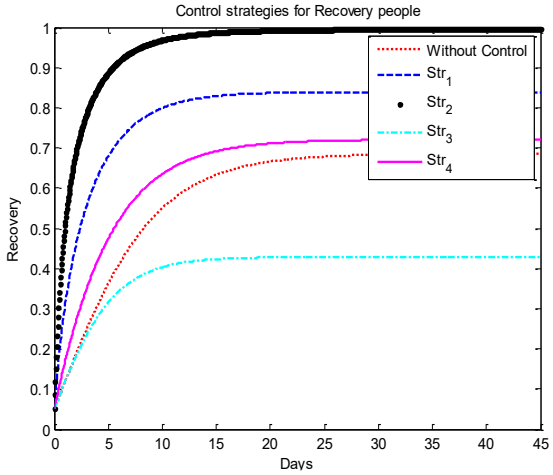

Fig. 19. Recovery individuals with control strategies

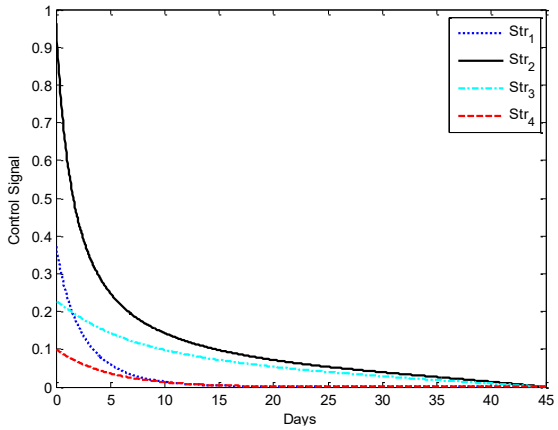

Fig. 20. Comparative between all control strategies

To determine the optimal control strategy among these four, we have to calculate the Eefficiency Iindex (EI) as presented in Table 4 [8].

Table 4. Efficiency Index of SIR model with different strategies

	Efficiency Index %			
	Str_1	**Str_2**	**Str_3**	**Str_4**
Ssusceptible	46 %	89 %	75 %	83 %
Iinfected	40 %	81 %	40 %	54 %

$$EI = \left(1 - \frac{A_o}{A_C}\right) \times 100 \tag{41}$$

where A_o and A_C are the cumulated number of state individuals without and with control, respectively. we can conclude that Strategy 2 is the optimal strategy.

It's important to acknowledge that the effectiveness of vaccination control (Strategy (2)) can vary due to several factors, such as vaccine efficacy, coverage rates, the emergence of new variants, and vaccine hesitancy. However, overall, vaccination control has proven to be a highly effective approach in reducing susceptibility, preventing infection, and shortening recovery periods in a population. To summarize, the effectiveness of vaccination control stems from its ability to stimulate the immune system, provide long-lasting protection, decrease disease severity, contribute to herd immunity, control transmission, and adapt to emerging variants. These characteristics collectively establish vaccination control as a highly efficient strategy for combating infectious diseases and mitigating their impact on public health. Also, treatment control (Strategy (1)) and quarantine and vaccination control (Strategy (4)) tend to be more cost-effective due to their targeted approach, early intervention, and preventive nature. However, trade-offs exist between effectiveness and cost, such as upfront investment, coverage rates, long-term costs, and the broader economic impact. Evaluating these trade-offs is crucial in determining the most appropriate and cost-effective control strategies for specific infectious diseases and populations.

5. GUI of SIR Optimal Control Strategies

To easily comprehend and determine system performance by altering any of the parameters. The SIR mathematical model's optimal control for various control strategies is investigated by the MATLAB program [59]-[61] with GUI shown in Fig. 21. These characteristics apply to this configuration:

- The ability to quickly enter data and modify variable values.
- The ability to choose the best possible control for the problem's and the infectious disease's type.
- The ability to enter new weights for the ideal controls for every strategy as needed to achieve the best outcomes.
- It is possible to study and follow the behavior of other infectious diseases that are most prevalent in reality, such Covid-19 disease, Ebola, and influenza.

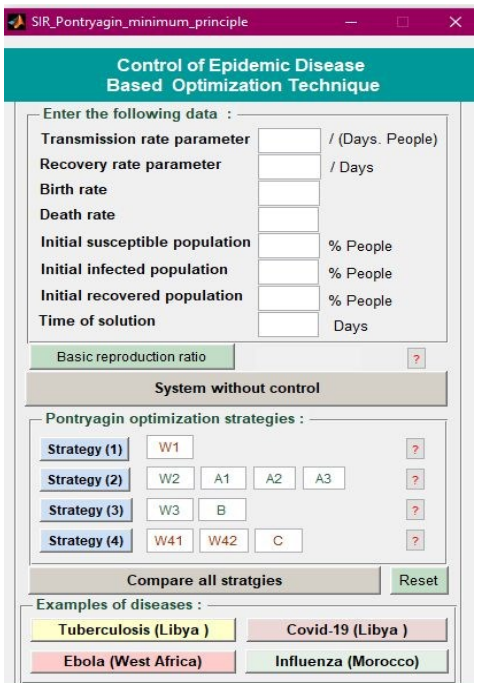

Fig. 21. GUI of SIR model for different diseases with optimal control [29]

The GUI for the SIR model offers a visual representation of disease dynamics, enabling users to observe the disease's spread over time. Interactive graphs and charts provide valuable insights into the progression of the epidemic, including the populations of susceptible, infectious, and recovered

individuals. Moreover, the GUI incorporates optimal control strategies, which involve identifying the most effective combination of interventions to minimize the disease's impact. By utilizing the GUI, users can evaluate the effectiveness of various strategies and make informed decisions based on data to determine the most efficient control measures. Additionally, the GUI allows for sensitivity analysis, enabling users to modify model parameters such as transmission rates, recovery rates, or the effectiveness of control measures. This functionality empowers researchers and policymakers to assess how the model's outcomes respond to changes in input parameters, thereby aiding in the evaluation of the model's sensitivity to different scenarios and variables.

6. Conclusion

In summary, this paper presents a versatile neural network-based model augmented by PMP control, offering a powerful tool for the analysis and effective control of infectious diseases. The development of a user-friendly graphical user interface (GUI) enhances its accessibility and usability. Notably, our approach emphasizes the adaptability of control strategies, allowing for customization based on various disease attributes, including emergence period, geographical origin, and underlying factors influencing transmission and recovery. By integrating diverse datasets, including population dynamics, our model yields context-specific and data-driven results. The primary objective function, optimized through the PMP approach, focuses on minimizing susceptibility and infection rates while maximizing recovery. This multi-faceted approach holds promise for optimizing disease control and mitigation strategies. The practical significance of our research lies in its potential to inform decision-makers in healthcare, public health, and policymaking. It offers a valuable tool for crafting tailored and effective responses to infectious disease outbreaks, ultimately minimizing their impact on communities and economies. Looking ahead, future research could explore extensions of our model and its application to a broader spectrum of infectious disease challenges. As we continue to grapple with the dynamics of infectious diseases, data-driven and adaptable approaches like ours will play a pivotal role in safeguarding public health.

Author Contribution: All authors contributed equally to the main contributor to this paper. All authors read and approved the final paper.

Funding: This research received no external funding.

Conflicts of Interest: The authors declare no conflicts of interest.

References

[1] N. S. Barlow and S. J. Weinstein, "Accurate closed-form solution of the SIR epidemic model," *Physica D: Nonlinear Phenomena*, vol. 408, p. 132540, 2020, https://doi.org/10.1016/j.physd.2020.132540.

[2] M. Pájaro, N. M. Fajar, A. Alonso, and I. Otero-Muras, "Stochastic SIR model predicts the evolution of COVID-19 epidemics from public health and wastewater data in small and medium-sized municipalities: A one year study," *Chaos, Solitons & Fractals*, vol. 164, p. 112671, 2022, https://doi.org/10.1016/j.chaos.2022.112671.

[3] Z. Shen, Y.-M. Chu, M. A. Khan, S. Muhammad, O. Al-Hartomy, and M. Higazy, "Mathematical modeling and optimal control of the COVID-19 dynamics," *Results in Physics*, vol. 31, p. 105028, 2021, https://doi.org/10.1016/j.rinp.2021.105028.

[4] M. Diagne, H. Rwezaura, S. Tchoumi, and J. Tchuenche, "A Mathematical Model of COVID-19 with Vaccination and Treatment," *Computational and Mathematical Methods in Medicine*, vol. 2021, pp. 1-16, 2021, https://doi.org/10.1155/2021/1250129.

[5] A. Abougarair, M. Aburakhis, and M. Edardar, "Adaptive Neural Networks Based Robust Output Feedback Controllers for Nonlinear Systems," *International Journal of Robotics and Control Systems*, vol. 2, no. 1, pp. 37-56, 2022, https://doi.org/10.31763/ijrcs.v2i1.523.

[6] S. Ullah and M. A. Khan, "Modeling the impact of non-pharmaceutical interventions on the dynamics of novel coronavirus with optimal control analysis with a case study," *Chaos, Solitons & Fractals*, vol. 139, p. 110075, 2020, https://doi.org/10.1016/j.chaos.2020.110075.

[7] T. Li and Y. Xiao, "Optimal strategies for coordinating infection control and socio-economic activities," *Mathematics and Computers in Simulation*, vol. 207, pp. 533–555, 2023, https://doi.org/10.1016/j.matcom.2023.01.017.

[8] J. Agbomola and A. Loyinmi, "Modelling the impact of some control strategies on the transmission dynamics of Ebola virus in human-bat population: An optimal control analysis," *Heliyon*, vol. 8, no. 12, p. e12121, 2022, https://doi.org/10.1016/j.heliyon.2022.e12121.

[9] G. Goswami and T. Labib, "Modeling COVID-19 Transmission Dynamics: A Bibliometric Review," *International Journal of Environmental Research and Public Health*, vol. 19, no. 21, p. 14143, 2022, https://doi.org/10.3390/ijerph192114143.

[10] I. Rahimi, A. Gandomi, P. Asteris, and F. Chen, "Analysis and Prediction of COVID-19 Using SIR, SEIQR, and Machine Learning Models: Australia, Italy, and UK Cases," *Information*, vol. 12, no. 3, p. 109, 2021, https://doi.org/10.3390/info12030109.

[11] Y. Zhi, W. Weiqing, C. Jing, and N. Razmjooy, "Interval linear quadratic regulator and its application for speed control of DC motor in the presence of uncertainties," *ISA Transactions*, vol. 125, pp 252–259, 2022, https://doi.org/10.1016/j.isatra.2021.07.004.

[12] J. Yang, Z. Chen, Y. Tan, Z. Liu, and R. Cheke, "Threshold dynamics of an age-structured infectious disease model with limited medical resources," *Mathematics and Computers in Simulation*, vol. 214, pp. 114–132, 2023, https://doi.org/10.1016/j.matcom.2023.07.003.

[13] D. I. Ketcheson, "Optimal control of an SIR epidemic through finite-time non-pharmaceutical intervention," *Journal of Mathematical Biology*, vol. 83, no. 1, 2021, https://doi.org/10.1007/s00285-021-01628-9.

[14] M. De la Sen, R. Nistal, S. Alonso-Quesada, and A. Ibeas, "Some Formal Results on Positivity, Stability, and Endemic Steady-State Attainability Based on Linear Algebraic Tools for a Class of Epidemic Models with Eventual Incommensurate Delays," *Discrete Dynamics in Nature and Society*, vol. 2019, p. e8959681, 2019, https://doi.org/10.1155/2019/8959681.

[15] L. Pujante-Otalora, B. Canovas-Segura, M. Campos, and J. M. Juarez, "The use of networks in spatial and temporal computational models for outbreak spread in epidemiology: A systematic review," *Journal of Biomedical Informatics*, vol. 143, p. 104422, 2023, https://doi.org/10.1016/j.jbi.2023.104422.

[16] J. E. Amaro, "Systematic description of COVID-19 pandemic using exact SIR solutions and Gumbel distributions," *Nonlinear Dynamics*, vol. 111, no. 2, pp. 1947–1969, 2022, https://doi.org/10.1007/s11071-022-07907-4.

[17] M. Abujarir, A. Abougarair, and H. Tarek "Artificial pancreas control using optimized fuzzy logic based genetic algorithm," *International Robotics & Automation Journal*, vol. 9, pp. 89-97, 2023. https://medcraveonline.com/IRATJ/IRATJ-09-00270.pdf.

[18] A. Kumar, K. Goel, and Nilam, "A deterministic time-delayed SIR epidemic model: mathematical modeling and analysis," *Theory in Biosciences*, vol. 139, no. 1, pp. 67–76, 2019, https://doi.org/10.1007/s12064-019-00300-7.

[19] L. Bai, J. J. Nieto, and J. M. Uzal, "On a delayed epidemic model with non-instantaneous impulses," *Communications on Pure & Applied Analysis*, vol. 19, no. 4, pp. 1915–1930, 2020, https://doi.org/10.3934/cpaa.2020084.

[20] M. De la Sen, A. Ibeas, S. Alonso-Quesada, and R. Nistal, "On a SIR Model in a Patchy Environment Under Constant and Feedback Decentralized Controls with Asymmetric Parameterizations," *Symmetry*, vol. 11, no. 3, p. 430, 2019, https://doi.org/10.3390/sym11030430.

[21] M. De la Sen, S. Alonso-Quesada, A. Ibeas, and R. Nistal, "On a Discrete SEIR Epidemic Model with Two-Doses Delayed Feedback Vaccination Control on the Susceptible," *Vaccines*, vol. 9, no. 4, p. 398, 2021, https://doi.org/10.3390/vaccines9040398.

[22] M. De, S. Alonso-Quesada, S. M. Muyeen, and R. Nistal, "On an SEIADR epidemic model with vaccination, treatment and dead-infectious corpses removal controls," *Mathematics and Computers in Simulation*, vol. 163, pp. 47–79, 2019, https://doi.org/10.1016/j.matcom.2019.02.012.

[23] K. Goel, A. Kumar, and Nilam, "Nonlinear dynamics of a time-delayed epidemic model with two explicit aware classes, saturated incidences, and treatment," *Nonlinear Dynamics*, vol. 101, no. 3, pp. 1693–1715, 2020, https://doi.org/10.1007/s11071-020-05762-9.

[24] S. Feng and Z. Jin, "Infectious Diseases Spreading on an Adaptive Metapopulation Network," *IEEE Access*, vol. 8, pp. 153425-153435, 2020, https://doi.org/10.1109/ACCESS.2020.3016016.

[25] A. Dababneh, N. Djenina, A. Ouannas, G. Grassi, I. M. Batiha, and I. H. Jebril, "A New Incommensurate Fractional-Order Discrete COVID-19 Model with Vaccinated Individuals Compartment," *Fractal and Fractional*, vol. 6, no. 8, p. 456, 2022, https://doi.org/10.3390/fractalfract6080456.

[26] Z.-Y. He, A. Abbes, H. Jahanshahi, N. D. Alotaibi, and Y. Wang, "Fractional-Order Discrete-Time SIR Epidemic Model with Vaccination: Chaos and Complexity," *Mathematics*, vol. 10, no. 2, p. 165, 2022, https://doi.org/10.3390/math10020165.

[27] D. Ghosh and R. K. De, "Block Search Stochastic Simulation Algorithm (BlSSSA): A Fast Stochastic Simulation Algorithm for Modeling Large Biochemical Networks," *IEEE/ACM Transactions on Computational Biology and Bioinformatics*, vol. 19, no. 4, pp. 2111-2123, 2022, https://doi.org/10.1109/TCBB.2021.3070123.

[28] Z. Shen, Y. Chu, M. Khan, S. Muhammad, O. Al-Hartomy, and M. Higazy, "Mathematical modeling and optimal control of the COVID-19 dynamics," *Results in Physics*, vol. 31, p. 105028, 2021, https://doi.org/10.1016/j.rinp.2021.105028.

[29] S. Elwefati, A. Abougarair and M. Bakush, "Control of Epidemic Disease Based Optimization Technique," *2021 IEEE 1st International Maghreb Meeting of the Conference on Sciences and Techniques of Automatic Control and Computer Engineering MI-STA*, pp. 52-57, 2021, https://doi.org/10.1109/MI-STA52233.2021.9464453.

[30] M. Sen and A. Ibeas, "On an Sir Epidemic Model for the COVID-19 Pandemic and the Logistic Equation," *Discrete Dynamics in Nature and Society*, vol. 2020, pp. 1–17, 2020, https://doi.org/10.1155/2020/1382870.

[31] N. Semendyaeva, M. Orlov, R. Tang, and Y. Enping, "Analytical and Numerical Investigation of the SIR Mathematical Model," *Computational Mathematics and Modeling*, vol. 33, pp. 284-299, 2023, https://doi.org/10.1007/s10598-023-09572-7.

[32] A. J. Abougarair, "Adaptive Neural Networks Based Optimal Control for Stabilizing Nonlinear System," *2023 IEEE 3rd International Maghreb Meeting of the Conference on Sciences and Techniques of Automatic Control and Computer Engineering (MI-STA)*, pp. 141-148, 2023, https://doi.org/10.1109/MI-STA57575.2023.10169340.

[33] H. Khodabandehlou and M. Fadali, "Nonlinear System Identification using Neural Networks and Trajectory-based Optimization," *Proceedings of the 16th International Conference on Informatics in Control, Automation and Robotics*, vol. 1, pp. 579-586, 2019, https://doi.org/10.5220/0007772605790586.

[34] A. Abougarair, "Neural Networks Identification and Control of Mobile Robot Using Adaptive Neuro Fuzzy Inference System," *Proceedings of the 6th International Conference on Engineering & MIS 2020*, vol. 1, pp. 579-586, 2020, https://doi.org/10.1145/3410352.3410734.

[35] C. Liu, P. Chen, Q. Jia, and L. Cheung, "Effects of Media Coverage on Global Stability Analysis and Optimal Control of an Age-Structured Epidemic Model with Multi-Staged Progression," *Mathematics,* vol. 10, no. 15, p. 2712, 2022, https://doi.org/10.3390/math10152712.

[36] A. Abougarair, "Optimal Control Synthesis of Epidemic Model," *IJEIT International Journal on Engineering and Information Technology*," vol. 8, no. 2, pp. 109-115, 2022, http://ijeit.misuratau.edu.ly/number-01-december-2022/.

[37] S. Margenov, N. Popivanov, I. Ugrinova, and T. Hristov, "Mathematical Modeling and Short-Term Forecasting of the COVID-19 Epidemic in Bulgaria: SEIRS Model with Vaccination," *Mathematics*, vol. 10, no. 15, p. 2570, 2022, https://doi.org/10.3390/math10152570.

[38] C. Hsu and J. Lin, "Stability of traveling wave solutions for a spatially discrete SIS epidemic model," *Zeitschrift für angewandte Mathematik und Physik*, vol. 70, no. 2, 2019, https://doi.org/10.1007/s00033-019-1107-1.

[39] N. Abuelezam, I. Michel, B. D. Marshall, and S. Galea, "Accounting for historical injustices in mathematical models of infectious disease transmission: An analytic overview," *Epidemics,* vol. 43, p. 100679, 2023, https://doi.org/10.1016/j.epidem.2023.100679.

[40] J. Giral-Barajas, C. I. Herrera-Nolasco, M. A. Herrera-Valdez, and S. I. López, "A probabilistic approach for the study of epidemiological dynamics of infectious diseases: Basic model and properties," *Journal of Theoretical Biology*, vol. 572, p. 111576, 2023, https://doi.org/10.1016/j.jtbi.2023.111576.

[41] M. Zhang and L. Zhang, "An optimal control problem for a biological population model with diffusion and infectious disease," *European Journal of Control*, vol. 72, p. 100821, 2023, https://doi.org/10.1016/j.ejcon.2023.100821.

[42] A. Kumar, A. Gupta, U. Dubey, and B. Dubey, "Stability and bifurcation analysis of an infectious disease model with different optimal control strategies," *Mathematics and Computers in Simulation*, vol. 213, pp. 78–114, 2023, https://doi.org/10.1016/j.matcom.2023.05.024.

[43] P. Jia, J. Yang, and X. Li, "Optimal control and cost-effective analysis of an age-structured emerging infectious disease model," *Infectious Disease Modelling*, vol. 7, no. 1, pp. 149-169, 2022, https://doi.org/10.1016/j.idm.2021.12.004.

[44] K. Guo *et al*., "Traffic Data-Empowered XGBoost-LSTM Framework for Infectious Disease Prediction," *IEEE Transactions on Intelligent Transportation Systems*, pp. 1-12, 2022, https://doi.org/10.1109/TITS.2022.3172206.

[45] S. Akbarian *et al*., "A Computer Vision Approach to Identifying Ticks Related to Lyme Disease," *IEEE Journal of Translational Engineering in Health and Medicine*, vol. 10, pp. 1-8, 2022, https://doi.org/10.1109/JTEHM.2021.3137956.

[46] M. Saeed, M. Ahsan, A. Mehmood, M. Saeed, and J. Asad, "Infectious Diseases Diagnosis and Treatment Suggestions Using Complex Neuromorphic Hyper Soft Mapping," *IEEE Access*, vol. 9, p. 146730-146744, 2021, https://doi.org/10.1109/ACCESS.2021.3123659.

[47] M. Kröger and R. Schlickeiser, "Analytical solution of the SIR-model for the temporal evolution of epidemics. Part A: time-independent reproduction factor," *Journal of Physics A: Mathematical and Theoretical*, vol. 53, no. 50, p. 505601, 2020, https://doi.org/10.1088/1751-8121/abc65d.

[48] M. Kröger, M. Turkyilmazoglu, and R. Schlickeiser, "Explicit formulae for the peak time of an epidemic from the SIR model. Which approximant to use?," *Physica D. Nonlinear Phenomena*, vol. 425, p. 132981, 2021, https://doi.org/10.1016/j.physd.2021.132981.

[49] S. Mungkasi, "Improved Variational Iteration Solutions to the SIR Model of Dengue Fever Disease for the Case of South Sulawesi," *Journal of Mathematical and Fundamental Sciences*, vol. 52, no. 3, pp. 297–311, 2020, https://doi.org/10.5614/j.math.fund.sci.2020.52.3.4.

[50] A. Abougarair, M. Ellafi, A. Ma'arif, and O. Salih, "Analysis of Mobile Accelerometer Sensor Movement Using Machine Learning Algorithm," *IEEE 3rd International Maghreb Meeting of the Conference on Sciences and Techniques of Automatic Control and Computer Engineering (MI-STA)*, pp. 46-51, 2023, https://doi.org/10.1109/MI-STA57575.2023.10169214.

[51] D. Cui, W. Zou, J. Guo, and Z. Xiang, "Neural network-based adaptive finite-time tracking control of switched nonlinear systems with time-varying delay," *Applied Mathematics and Computation*, vol. 428, p. 127216, 2022, https://doi.org/10.1016/j.amc.2022.127216.

[52] A. S. Elmulhi and A. J. Abougarair, "Sliding Mode Control for the Satellite with the Influence of Time Delay," *2023 IEEE 3rd International Maghreb Meeting of the Conference on Sciences and Techniques of Automatic Control and Computer Engineering (MI-STA)*, pp. 77-82, 2023, https://doi.org/10.1109/MI-STA57575.2023.10169804.

[53] A. Abougarair and A. Elmulhi, "Robust control and optimized parallel control double loop design for mobile robot," *International Journal of Robotics and Automation (IJRA)*, vol. 9, pp. 160-170, 2020. https://doi.org/10.11591/ijra.v9i3.pp160-170.

[54] Y. Qiu, Y. Li, and Z. Wang, "Robust Near-optimal Control for Constrained Nonlinear System via Integral Reinforcement Learning," *International Journal of Control Automation and Systems*, vol. 21, no. 4, pp. 1319–1330, 2023, https://doi.org/10.1007/s12555-021-0674-z.

[55] P. Subbash and K. T. Chong, "Adaptive network fuzzy inference system-based navigation controller for mobile robot," *Frontiers of Information Technology & Electronic Engineering*, vol. 20, no. 2, pp. 141-151, 2019, https://doi.org/10.1631/FITEE.1700206.

[56] C. J. Luis Pérez, "A Proposal of an Adaptive Neuro-Fuzzy Inference System for Modeling Experimental Data in Manufacturing Engineering," *Mathematics*, vol. 8, no. 9, p. 1390, 2020, https://doi.org/10.3390/math8091390.

[57] A. Abougarair, N. Shashoa, and M. Aburakhis, "Performance of Anti-Lock Braking Systems Based on Adaptive and Intelligent Control Methodologies," *Indonesian Journal of Electrical Engineering and Informatics (IJEEI)*, vol. 10, no. 3, 2022, https://doi.org/10.52549/ijeei.v10i3.3794.

[58] M. Barro, A. Guiro, and D. Ouedraogo, "Optimal control of a SIR epidemic model with general incidence function and a time-delays," *Cubo (Temuco)*, vol. 20, no. 2, pp. 53–66, 2018, https://doi.org/10.4067/S0719-06462018000200053.

[59] F. Shults and W. Wildman, "Human Simulation and Sustainability: Ontological, Epistemological and Ethical Reflections," *Sustainability*, vol. 12, no. 23, p. 10039, 2020, https://doi.org/10.3390/su122310039.

[60] A. Ma'arif, M. Antonio, M. Sadek, E. Umoh, and A. Abougarair, "Sliding Mode Control Design for Magnetic Levitation System", *Journal of Robotics and Control (JRC)*, vol. 3, no 6, pp. 848-853, 2022, https://doi.org/10.18196/jrc.v3i6.12389.

[61] A. J. Abougarair and N. A. A. Shashoa, "Model Reference Adaptive Control for Temperature Regulation of Continuous Stirred Tank Reactor," *2021 IEEE 2nd International Conference on Signal, Control and Communication (SCC)*, pp. 276-281, 2021, https://doi.org/10.1109/SCC53769.2021.9768396.